Accelerating the Kinetics of Thiol Self-Assembly on Gold—A Spatial Confinement Effect

Song Xu,† Paul E. Laibinis,‡ and Gang-yu Liu*,†

Contribution from the Department of Chemistry, Wayne State University, Detroit, Michigan 48202, and Department of Chemical Engineering, Massachusetts Institute of Technology, Cambridge, Massachusetts 02139

Received June 3, 1998

Abstract: The adsorption of alkanethiols onto gold surfaces to form self-assembled monolayers (SAMs) occurs more than 10 times faster in a spatially confined environment than on unconfined bare substrates, and the adsorbed layers exhibit higher coverage and two-dimensional crystallinity. The spatially constrained reaction environment is prepared with use of an atomic force microscope tip to displace thiols within a previously formed SAM. During the displacement, the thiol molecules present in the solution above the SAM rapidly assemble onto the exposed nanometer-size gold area that is confined by the scanning tip and surrounding SAM. The accelerated rate is attributed to a change in the pathway for the self-assembly process as the spatial confinement makes it geometrically more probable and energetically more favorable for the initially adsorbed thiols to adopt a standing-up configuration directly in this microenvironment. In contrast, thiols that self-assemble onto gold surfaces in an unconstrained environment initially form a lying-down phase, which subsequently degrades and forms a standing-up phase. Our observations suggest that spatial confinement can provide an effective means to change the mechanism and kinetics of certain surface reactions by sterically preventing alternative reaction pathways and stabilizing particular transition states or reaction intermediates. In addition, the results underlie the development of a new method ("nanografting") for patterning SAMs laterally with nanometer-level precision.

Introduction

Self-assembled monolayers (SAMs) offer many promising applications in the developments of boundary lubricants, anticorrosion coatings, and recently the microfabrication process because they can be laterally patterned and then used as resists for pattern transfer.[1−3] To be effective as a resist, the SAM should be stable and contain few defects. A popular system for these applications has been SAMs derived from the adsorption of alkanethiols onto metals such as gold, silver, and copper.[4] These thiol-derived SAMs contain ordered domains that are separated by boundaries (areas of lower surface coverage) and various defects,[1,5,6] whose size and distribution depend on the interplay of kinetic and thermodynamic factors during the growth of the SAM. Empirically, a thiol-derived SAM with a large domain size and low defect density can be prepared by contacting a gold surface with a dilute solution of the thiol for at least 24 h.[1,4,7] A molecular level understanding of the self-assembly process and kinetics is of fundamental importance for improving the quality and usefulness of SAMs.

As shown in recent studies using scanning tunneling microscopy (STM)[8] and helium and X-ray diffraction,[9] the self-assembly of these molecules from the vapor phase follows two major steps. First, the thiol molecules adsorb on gold and form a lattice-gas or mobile phase that gradually evolves into crystalline islands with the molecules oriented parallel to the gold surface.[8,9] At the saturation coverage of this lying-down phase, a solid-to-solid-phase transition occurs to produce islands of molecules in a standing-up configuration.[8] Using low-energy helium diffraction, Schwartz et al. revealed that the low-density lying-down monolayer degrades into a disordered state, from which the standing-up phase is formed.[9] Using an ultrahigh vacuum STM, Poirier and Pylant provided a molecular-level *in situ* picture at each step of the self-assembly process for thiols onto gold from the vapor phase.[8] In practice, most SAMs are prepared from a solution phase.[1,4] Under these conditions,

* To whom correspondence should be addressed.
† Wayne State University.
‡ Massachusetts Institute of Technology.

(1) Ulman, A. *An Introduction to Ultrathin Organic Films—From Langmuir−Blodgett to Self-Assembly*; Academic Press: San Diego, 1991.
(2) (a) Wollman, E. W.; Kang, D.; Frisbie, C. D.; Lorkovic, I. M.; Wrighton, M. S. *J. Am. Chem. Soc.* **1994**, *116*, 4395. (b) Huang, J. Y.; Dahlgren, D. A.; Hemminger, J. C. *Langmuir* **1994**, *10*, 626. (c) Tarlov, M. J.; Burgess, D. R. F.; Gillen, G. *J. Am. Chem. Soc*. **1993**, *115*, 5305.
(3) (a) Kumar, A.; Whitesides, G. M. *Science* **1994**, *263*, 60. (b) Xia, Y.; Whitesides, G. M. *J. Am. Chem. Soc*. **1995**, *117*, 3274. (c) Jeon, N. L.; Nuzzo, R. G.; Xia, Y.; Mrksich, M.; Whitesides, G. M. *Langmuir* **1995**, *11*, 3024.
(4) (a) Nuzzo, R. G.; Allara, D. L. *J. Am. Chem. Soc.* **1983**, *105*, 448. (b) Laibinis, P. E.; Whitesides, G. M.; Allara, D. L.; Tao, Y.-T.; Parikh, A. N.; Nuzzo, R. G. *J. Am. Chem. Soc*. **1991**, *113*, 7152.
(5) (a) Poirier, G. E.; Tarlov, M. J. *Langmuir* **1994**, *10*, 2853. (b) Poirier, G. E.; Tarlov, M. J.; Rushmeierf, H. E.; *Langmuir* **1994**, *10*, 3383. (c) Sondag-Huthorst, J. A. M.; Schönenberger, C.; Fokkink, L. G. *J. Phys. Chem*. **1994**, *98*, 6826. (d) McDermott, C. A.; McDermott, M. T.; Green, J. B.; Porter, M. D. *J. Phys. Chem*. **1995**, *99*, 13257. (e) Bucher, J. P.; Santesson, L.; Kern, K. *Langmuir* **1994**, *10*, 979.
(6) (a) Camillone, N. C.; Chidsey, C. E. D.; Liu, G. Y.; Scoles, G. *J. Chem. Phys*. **1993**, *98*, 3503. (b) Camillone, N.; Chidsey, C. E. D.; Liu, G. Y.; Scoles, G. *J. Chem. Phys*. **1993**, *98*, 4234. (c) Fenter, P.; Eberhardt, A.; Liang, K. S.; Eisenberger, P. *J. Chem. Phys*. **1997**, *106*, 1600.
(7) (a) Karpovich, D. S.; Blanchard, G. J. *Langmuir* **1994**, *10*, 3315. (b) Peterlinz, K. A.; Georgiadis, R. *Langmuir* **1996**, *12*, 4731.
(8) Poirier, G. E.; Pylant, E. D. *Science* **1996**, *272*, 1145.
(9) (a) Camillone, N.; Leung, T. Y. B.; Schwartz, P.; Eisenberger, P.; Scoles, G. *Langmuir* **1996**, *12*, 2737. (b) Schwartz, P.; Schreiber, F.; Eisenberger, P.; Scoles, G. *Phys. Rev. B* **1998**, preprint.

S0002-7863(98)01938-6 CCC: $15.00
Published on Web 08/20/1998

atomic force microscopy (AFM) allows surface reactions be followed *in situ* and in real time with high spatial resolution.[10] In a previous study, we examined the mechanism and kinetics of self-assembly in solution using time-dependent AFM images acquired during the formation of SAMs.[10] This work revealed a stepwise process for the formation of the SAM and the presence of a structural phase transition during its assembly.[10]

In general, chemical reactions can be accelerated by increases in the concentration of reactants and in the reaction temperature, or by using catalysts which often change the reaction mechanism. In certain gas-phase and solution-phase reactions, rate accelerations have been possible within microscopic environments such as the cavities of zeolites, and the capsules of proteins and various supramolecular complexes.[11] The rate enhancements for these systems often result from the existence of encapsulating microenvironments that enthalpically stabilize specific reaction intermediates and may sterically favor the formation of a particular product.[11] For the reaction processes that underlie the self-assembly of thiols onto gold to form densely packed monolayers, these processes can be accelerated by increases in the concentration of thiols or in the reaction temperature, or by changes in the polarity of the solvent medium.[1,7,10] In general, the layers formed at these accelerated rates typically have small domain sizes and high defect densities. In the present study, we reveal that the self-assembly process is accelerated within a spatially confined environment and proceeds without sacrificing the quality of the resulting monolayer. The spatially confined environment is produced during a fabrication process called nanografting[12] in which a gold surface is spatially confined by surrounding adsorbed thiols and an AFM tip. We have systematically investigated and compared the kinetics of self-assembly of thiols from solution onto freshly prepared gold surfaces and under spatially confined conditions. When the exposed gold area is sufficiently small, the process for SAM formation is at least 10 times faster than the corresponding unconfined process. In addition, SAMs formed under such spatial constraint have a higher coverage and crystallinity than the corresponding layers formed on an unconstrained gold surface. These observations appear to reflect a change in the self-assembly pathway that directly results from the spatial confinement.

Experimental Method

The AFM employs a home-constructed, deflection-type scanning head that exhibits high mechanical stability and a liquid cell that allows injection of solutions with minimal disturbance during in situ imaging.[10] The scanner was controlled by an AFM100 preamplifier and STM1000 electronics manufactured by RHK Technology. Sharpened Si_3N_4 microlevers (Park Scientific Instruments) with a force constant of 0.1 N/m were used for AFM imaging.

Gold (Alfa Aesar, 99.999%) was deposited in a high-vacuum evaporator (Denton Vacuum Inc., Model DV502-A) at a base pressure of ca. 10^{-7} Torr onto freshly cleaved mica substrates (clear ruby muscovite, Mica New York Corp.). The mica was preheated to 325 °C before deposition by using two quartz lamps mounted behind the mica to enhance the formation of terraced Au(111) domains.[13] Typical evaporation rates were 3 Å/s, and the thickness of the gold films ranged from 1500 to 2000 Å.

n-Alkanethiols $CH_3(CH_2)_nSH$ (abbreviated to $C_{n+1}SH$) were purchased from Aldrich and used as received, except for 1-docosanethiol ($C_{22}SH$) and 19-(octadecyloxy)nonadecanethiol ($C_{18}OC_{19}SH$) that were available from a previous study.[10]

Results and Discussion

Self-Assembly of Alkanethiols from Solution onto Gold Surfaces. Figure 1 displays nine selected images representing critical moments during the self-assembly of $C_{18}SH$ from a 0.2 mM solution onto a freshly prepared gold thin film. Initially, the adsorbed thiol molecules align parallel to the surface (see Figure 1, parts B, B′, C, and C′). As adsorption proceeds, elevated islands ranging from 20 to 100 Å in lateral dimension appear in image 1D, where the height difference between these islands and the lying-down phase is 15 ± 2 Å (Figure 1D′). The height measurements in these topographic images suggest that these islands contain thiols in a standing-up configuration. With continued exposure to the thiols, the coverage of the standing-up phase increases through both nucleation and the growth of nuclei (Figure 1D−I). From this series of time-dependent in situ AFM images, we conclude that the self-assembly of thiols onto gold from solution follows a similar mechanism to that from the vapor phase as revealed from investigations using STM[8] and helium and X-ray diffraction.[9] In the 0.2 mM thiol solution, a nearly complete monolayer (∼95%) formed in ∼30 min and contained domains of close-packed thiol molecules[5,6] separated by "dark scars" that slowly heal over time periods of 24−96 h.[10] These scars are likely to be gold areas that are covered by weakly adsorbed species that became trapped during the growth of the SAM.

Self-Assembly of Alkanethiols onto Gold under Spatial Confinement. To study self-assembly under spatially constrained conditions, we follow a three-step process called nanografting.[12] First, AFM is used to image a previously formed monolayer (matrix SAM) in a solution containing a desired thiol, and then the tip is positioned at a selected site. Second, the load is slowly increased to slightly above the displacement threshold for thiol adsorbates.[14] During the scan, the AFM tip displaces the matrix thiols underneath the tip and exposes the Au(111) surface to the thiol solution;[15] we refer to this step as nanoshaving. This displacement creates a transient microenvironment in which the freshly exposed gold is spatially constrained by the surrounding thiols and the AFM tip. Self-assembly of thiols from solution onto the newly exposed gold areas occurs within this reaction environment to form a SAM. Finally, the growth of the new monolayer is monitored at a reduced imaging force.[12] For clarity, we refer to self-assembly that occurs during nanoshaving as spatially confined (or constrained) self-assembly (SCSA) and adsorption that occurs by immersing freshly prepared gold substrates into thiol solutions (as in Figure 1) as unconstrained self-assembly.

Nanografting experiments with a $C_{18}S$ matrix in a 0.2 mM $C_{18}SH$ solution (Figure 2) produced two important observations. First, SCSA occurs faster than unconstrained growth in common thiol solutions. From the images taken immediately before and after the nanoshaving step (Figure 2, parts A and B), SAMs formed in less than 2.5 min. Our experimental approach in this case was not sufficiently fast to follow the SCSA. Most likely,

(10) Xu, S.; Cruchon-Dupeyrat, S.; Garno, J.; Liu, G. Y.; Jennings, G. K.; Yong T.-H.; Laibinis, P. E. *J. Chem. Phys*. **1998**, *108*, 5002.

(11) (a) Tokuna, Y.; Rebek, J. *J. Am. Chem. Soc*. **1998**, *120*, 66. (b) Kang, J. M.; Rebek, J. *Nature* **1996**, *382*, 239.

(12) Xu, S.; Liu, G. Y. *Langmuir* **1997**, *13*, 127.

(13) (a) Hegner, M.; Wagner, P.; Semenza, G. *Surf. Sci*. **1993**, *291*, 39. (b) Wagner, P.; Hegner, M.; Guntherodt, H.-J.; Semenza, G. *Langmuir* **1995**, *11*, 3867. (c) Chidsey, C. E. D.; Loaicano, D. N.; Sleator, T.; Nakahaza, S. *Surf. Sci.* **1988**, *200*, 45. (d) Lang, C. A.; Dovek, M. M.; Nogami, J.; Quate, C. F. *Surf. Sci. Lett.* **1989**, *224*, 1974. (e) Wöll, Ch.; Chiang, S.; Wilson, R. J.; Lippel, P. H. *Phys. Rev. B* **1989**, *39*, 7988.

(14) (a) Liu, G. Y.; Salmeron, M. B. *Langmuir* **1994**, *10*, 367. (b) Liu, G. Y.; Fenter, P.; Eisenberger, P.; Chidsey, C. E. D.; Ogletree, D. F.; Salmeron, M. B. *J. Chem. Phys*. **1994**, *101*, 4301.

(15) The displaced thiols may dissolve into the solvent as RSSR, $RSAu_n$, RSH, or RSO_3^-.

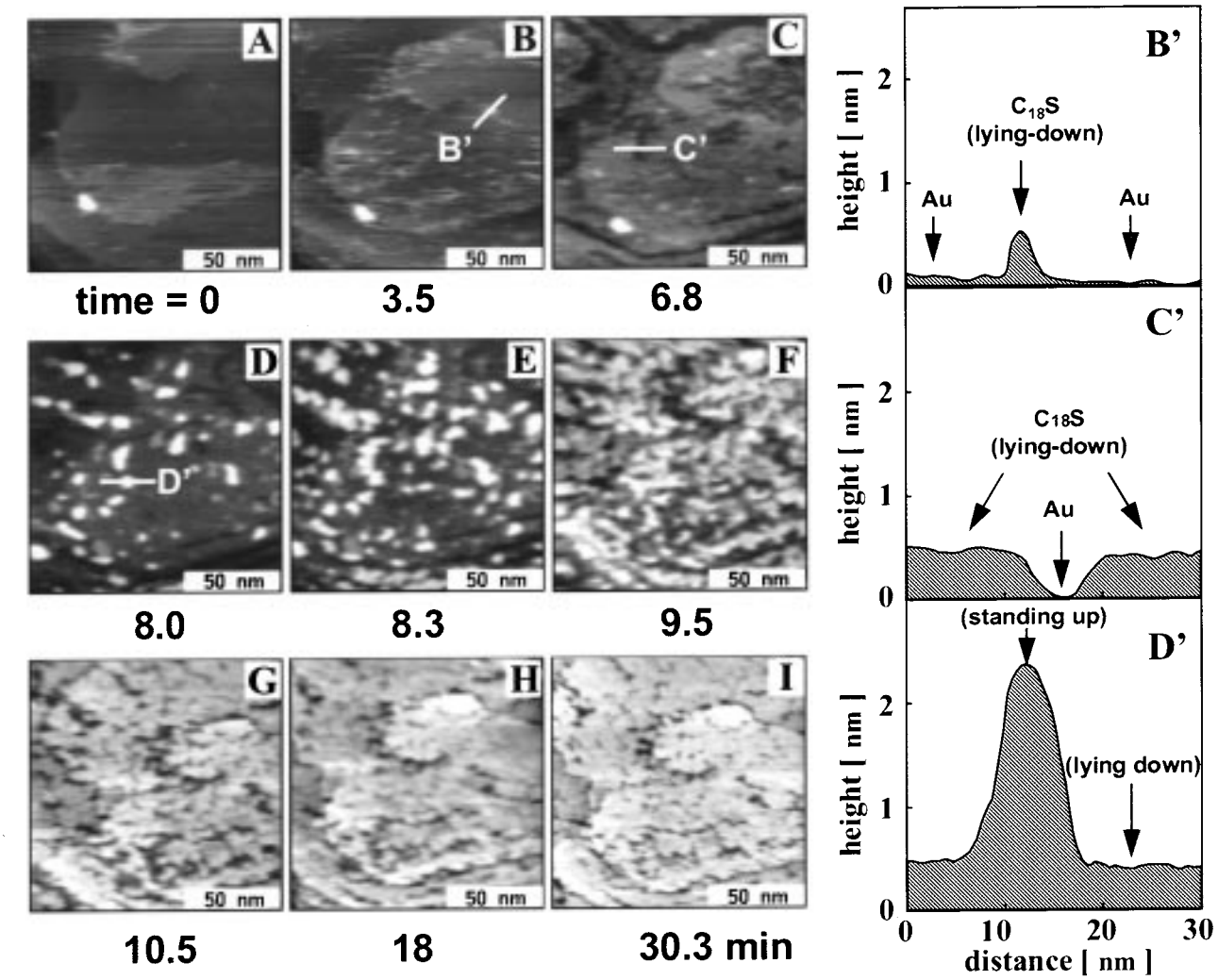

Figure 1. (A−I) In situ AFM images of the self-assembly of $C_{18}SH$ onto a freshly prepared Au(111) thin film from a 2-butanol solution. (B′−D′) Cross-sectional profiles for the corresponding line traces in images B−D. The concentration of $C_{18}SH$ was 0.2 mM. An elevated island (the bright spot) and several Au(111) single atomic steps in the lower left region of the image provided landmarks for *in situ* imaging.

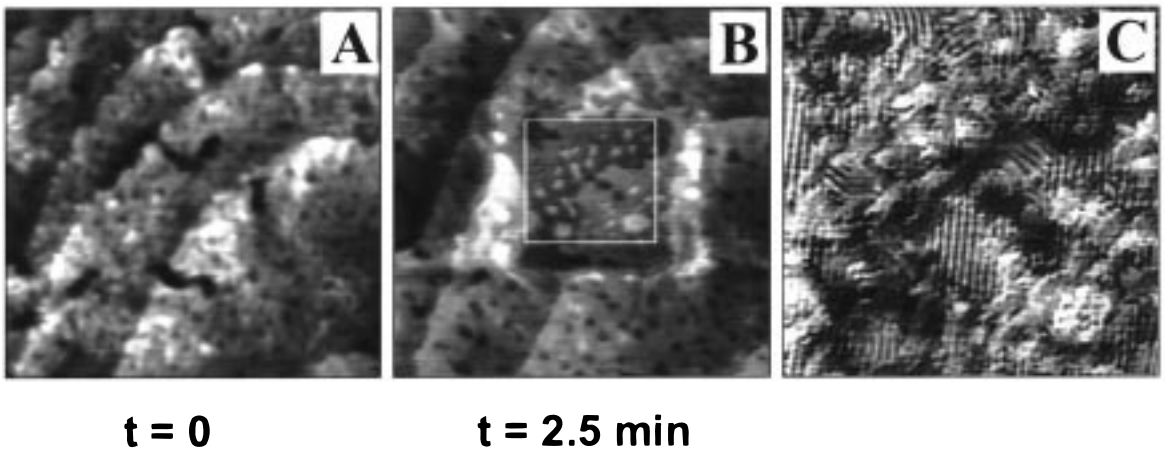

Figure 2. (A) A 150 × 150 nm^2 topographic scan of a $C_{18}S$ SAM at an imaging force of 0.1 nN. The Au(111) terraces are separated by five single-atom steps. (B) After nanografting in the central 50 × 50 nm^2 area with a displacement force of 1.2 nN and a speed of 250 nm/s in a 0.2 mM $C_{18}SH$ solution. Note that the scars in part A are absent in the central area in part B. The boundary between the matrix and grafted areas can be identified easily because of the structural discontinuity. Etch pits are more clearly resolved in (B) because the AFM tip is sharpened during the high force scan or shaving process. (C) High-resolution image acquired by zooming into the region indicated in (B).

adsorption occurred following the shaving track of the AFM tip. The second observation is the scar-free morphology and long-range order of the newly formed SAM. Image 2B reveals that this newly formed SAM exhibits a similar thickness and surface morphology as the surrounding matrix that was formed by soaking a gold thin film in a 1 mM thiol solution for at least 72 h. As a comparison, the monolayer formed on bare gold after soaking for 30 min in a 0.2 mM thiol solution (Figure 1I)

Table 1. Reaction Times (t) to Reach a Saturation Coverage (θ) during the Formation of Monolayers

unconstrained		spatially constrained		
reaction	t (min) for $\theta \approx 95\%$	reaction	t (min)[a] for $\theta \approx 100\%$	area (nm^2)
0.2 mM $C_{18}SH$ + Au(111)	30 ± 1	0.2 mM $C_{18}SH$ + Au(111) in		
		$C_{18}S$/Au(111)	<1.2	50 × 50
		$C_{10}S$/Au(111)	<2.0	$10^3 \times 10^3$
		$C_{10}S$/Au(111)	<1.8	20 × 70
		HOC_2S/Au(111)	<2.5	50 × 50
0.1 mM $C_{22}SH$ + Au(111)	30 ± 1	0.1 mM $C_{22}SH$ + Au(111) in		
		$C_{22}S$/Au(111)	<3.8	50 × 50
		$C_{18}S$/Au(111)	<3.0	50 × 50
		$C_{18}S$/Au(111)	<0.1	30 × 100
		$C_{10}S$/Au(111)	<2.5	$10^3 \times 10^3$
			≈0.1	30 × 100
		2 μM $C_{22}SH$ + Au(111) in		
		$C_{18}S$/Au(111)	<3.0	50 × 50
2 μM $C_{18}OC_{19}SH$ + Au(111)	50 ± 2	2 μM $C_{18}OC_{19}SH$ + Au(111) in		
		$C_{18}OC_{19}S$/Au(111)	<2.4	50 × 50

[a] The time was measured from the beginning of nanoshaving to the completion of the first image taken immediately after the shaving process. The actual self-assembly most likely occurred continuously following the shaving track of the AFM tip, and is therefore faster than the values in the table.

exhibited visible scars. From the same 0.2 mM thiol solution, the monolayer grown under spatial confinement (Figure 2B) is scar-free. In fact, the original scars in the central 50 × 50 nm^2 area (Figure 2A) are no longer present within the SAM formed during nanografting. In addition, the molecularly resolved image in Figure 2C reveals the presence of long-range order within the newly formed SAM. Most of the ordered domains are consistent with the c(4 × 2) superlattice with respect to the basic $(\sqrt{3}\times\sqrt{3})R30°$ periodicity for alkanethiol monolayers on Au(111).[5,6] In contrast to this image, previously reported high-resolution AFM images of SAMs show either perfectly ordered periodic molecular structures or defects on a larger scanning range,[14,16] but not the well-defined, laterally resolved molecular defects seen in STM images.[5,8] The sharpened AFM tip and small imaging force (~0.1 nN) made it possible to achieve the true molecular resolution in image 3C, as evidenced by the clear resolution of etch pits, vacancies, domain boundaries, and the superlattice.

The only difference between self-assembly in Figures 1 and 2 is the reaction environment. The bare gold surface was unconstrained in the former case and spatially constrained by the AFM tip and the surrounding thiols in the latter experiment. The above results suggest that such a transient microenvironment may have accelerated the self-assembly process (adsorption and ordering) and prevented the formation of scars. The acceleration effect was consistently observed when we systematically varied the size and geometry of the fabricated areas, and the chain length and terminal groups of the matrix and solution thiols as summarized in Table 1. Under conditions where the assembly of $C_{18}SH$, $C_{22}SH$, and $C_{18}OC_{19}SH$ onto bare gold took 30 to 50 min to form a nearly complete monolayer (a coverage greater than 95%), corresponding SCSA experiments produced scar-free SAMs of ~100% coverage within the time scale of one imaging−shaving−imaging cycle (~1 to 4 min). Such accelerated kinetics were observed even when the thiol concentration was reduced to micromolar levels (see Table 1). In all cases, SCSA occurred at least 1 order of magnitude faster than the corresponding unconstrained process.

There are several plausible alternative explanations for the faster kinetics in SCSA. Possible tip effects include that the AFM tip under high force guides the adsorption of thiols. Additionally, a cleaner and more reactive gold surface fabricated during nanografting could be responsible for the accelerated self-assembly process. Other explanations include a high rate of mass transfer of the thiols to the ultramicroscopic gold regions exposed during nanoshaving; this effect would be analogous to the high rate of mass transfer in the case of ultramicroelectrodes.[17] The following "blank" experiment was performed to test the above possibilities. First, a freshly prepared gold surface was immersed in a 0.2 mM $C_{18}SH$ solution. Immediately after the immersion, the imaging−shaving−imaging procedure (~2.5 min per cycle) was repeated using the same conditions as those in Figure 2. In this experiment, the AFM tip sequentially operated at a low load to image a 150 × 150 nm^2 area and a high load on randomly selected 50 × 50 nm^2 areas within the larger imaged region to displace adsorbates and produce clean gold areas. Initially, the surface consisted of bare gold (or more often gold covered with weakly adsorbed species). Nanoshaving on such surface could not generate the spatially confined environment. We observed that self-assembly on these 50 × 50 nm^2 areas exhibited the same mechanism and kinetics as on the surrounding unperturbed reaction sites. This observation suggests that the effect of the AFM tip operated under high force cannot account for the accelerated self-assembly processes. As the reaction proceeded, nanografting within the lying-down phase or a mixed layer of lying-down and standing-up molecules was still not successful due to the inability of these systems to produce the microenvironment that can be fabricated in a mature SAM (e.g. Figure 1 and Table 1). This observation also indicated that tip perturbation effect and diffusional factors were not mainly responsible for accelerating the growth of the SAM. Specifically, accelerated kinetics were observed during nanoshaving only after the standing-up phase reached a coverage of more than 80% and could provide the necessary microenvironment or sufficient spatial confinement.

To measure the rate of SCSA and further define the dimension of spatial confinement, we systematically investigated the formation of a SAM during the nanografting process as a function of the speed and total area of thiol displacement. Figure 3 shows an example of grafting $C_{22}SH$ patterns within a $C_{18}S$/Au(111) matrix. At a shaving rate of 250 nm/s (Figure 3, parts

(16) (a) Alves, C. A.; Smith, E. L.; Porter, M. D. *J. Am. Chem. Soc.* **1992**, *114*, 1222. (b) Butt, H. J.; Seifert, K.; Bamberg, E. *J. Phys. Chem.* **1993**, *97*, 7316.

(17) (a) Bard, A. J.; Abruna, H. D.; Chidsey, C. E. D.; Faulkner, L. R.; Feldberg, S. W.; Itaya, K.; Majda, M.; Melroy, O.; Murray, R. W.; Porter, M. D.; Soriaga, M. P.; White, H. S. *J. Phys. Chem.* **1993**, *97*, 7148. (b) Hulteen, J. C.; Menon, V. P.; Martin, C. R. *J. Chem. Soc., Faraday Trans.* **1996**, *92*, 4029.

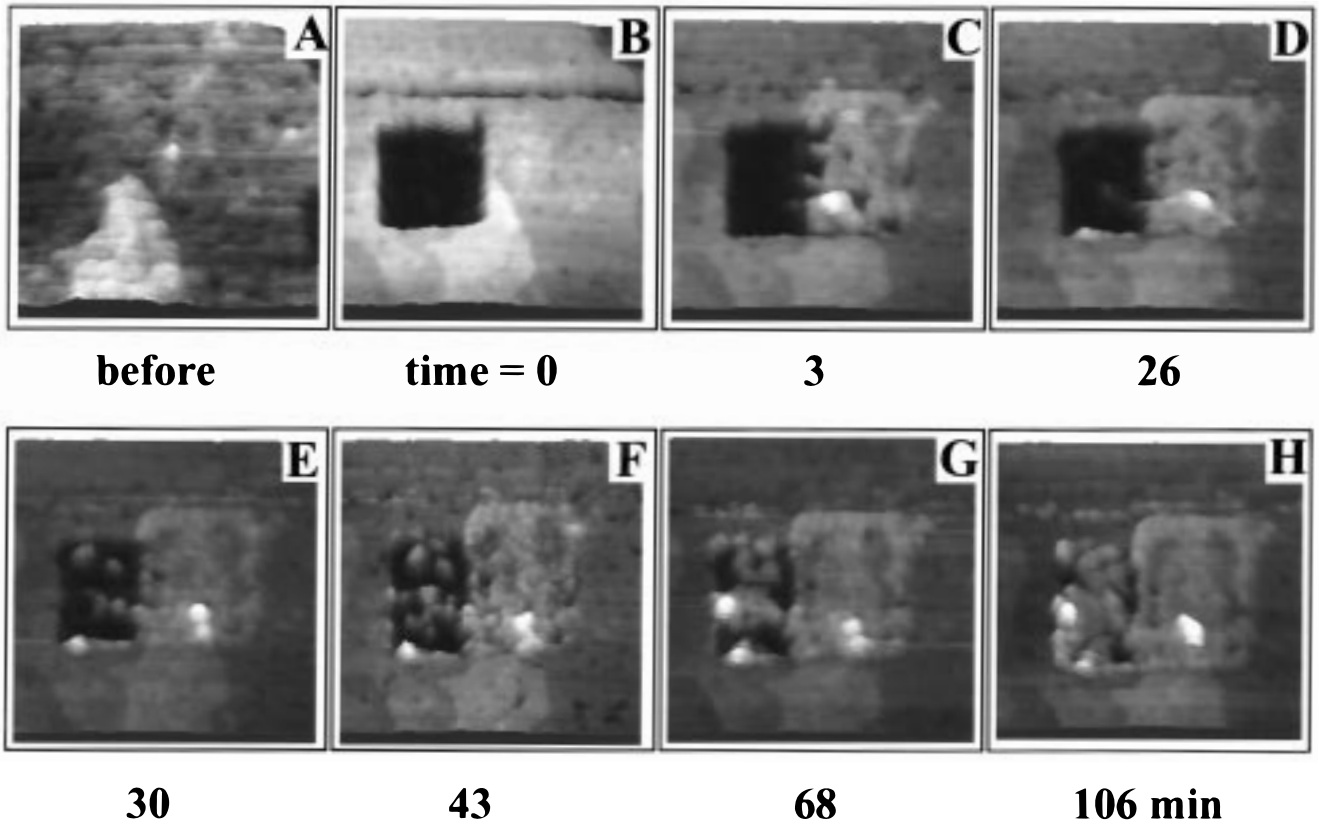

Figure 3. *In situ* time-dependent AFM images for the nanografting of $C_{22}SH$ from a 2 μM solution into a $C_{18}S$/Au(111) matrix at different speeds of $C_{18}S$ displacement. (A) $C_{18}S$/Au(111) before nanoshaving. (B) Adjacent regions of uncovered Au(111) surface (a 50 × 50 nm^2 square hole and a horizontal 2.0 × 150 nm^2 line) were produced at a shaving speed of 10 000 nm/s. (C) Successful grafting of a 50 × 50 nm^2 $C_{22}S$ island into a region adjacent to the square hole in (B) at a tip rate of 250 nm/s. Some imperfections appear at the left edge where the new region overlaps with the previous square hole. (D−H) Time-dependent AFM images showing the slow kinetics and growth mechanism of $C_{22}S$ SAM nuclei at the unconstrained square and partially confined line. The direction for imaging and nanografting was along the *x*-axis.

B and C), a 50 × 50 nm^2 region of $C_{22}S$ SAM formed in less than 2.5 min—an observation that is consistent with the kinetics of SCSA. Such accelerated kinetics were observed when the same procedure was repeated with higher shaving speeds, except at or above 10 000 nm/s, which produced a 50 × 50 nm^2 region of bare gold (Figure 3B). As clearly shown in parts B−H of Figure 3, self-assembly in this area followed the pathway and kinetics similar to the unconstrained process.[18] These observations indicate that the speed of SCSA in the case shown in Figure 3 is slightly slower than the threshold shaving speed of 10 000 nm/s, above which self-assembly changes from SCSA to the unconstrained pathway.

At a displacement rate of 10 000 nm/s, various nanoscopic reaction environments consisting of gold areas (holes) of different geometries could be produced, of which Figure 3 shows a 2 × 150 nm^2 line and a 50 × 50 nm^2 square hole. The kinetics of self-assembly into this line (B−D, Figure 3) were between those for the constrained (B and C, Figure 3) and unconstrained 50 × 50 nm^2 areas (B−H, Figure 3). Self-assembly on wider lines and the 50 × 50 nm^2 square hole followed similar rates to the unconstrained reactions. These observations suggest that the dimension of the microenvironment created during nanoshaving is critical for the acceleration in SAM formation. While scanning an AFM tip under a high force, small areas of gold become exposed that are enclosed along their perimeter by previously adsorbed thiols and the AFM tip. SCSA occurred within these regions when their opening of the holes was smaller than the chain length of the thiols in solution (e.g. 2.8 nm for $C_{22}SH$). In such a microenvironment, the initially adsorbed thiols adopted the standing-up configuration directly. This new pathway produces scar-free SAMs with high crystallinity because defects such as scars and domain boundaries form when nearby SAM nuclei grow and coalesce, as for self-assembly in an unconstrained environment.

Proposed Mechanism for the Acceleration in Self-Assembly during Nanografting. The accelerated kinetics in SCSA can be explained qualitatively by an altered reaction pathway, as schematically shown in Figure 4.[19] For unconstrained self-assembly, the reaction mechanism includes two steps with the lying-down phase as a reaction intermediate (Figure 4A). For SCSA, adsorption occurs within the transient

(18) Caution must be taken here as strongly adsorbed contamination on gold can extend the preadsorption period.[10]

(19) It is difficult to provide quantitative or even semiquantitative explanations due to the complexity of such surface reactions. Using transition state theory, one can qualitatively attribute the accelerated kinetics to the reduced activation energies in the SCSA reaction pathway. The fast kinetics in SCSA may also be explained using collision theory, where the rate constants for forming SAMs are estimated to be $FSf(\theta)\exp(-E_2^*/kT)$ and $F^*S^*f^*(\theta)\exp(-E_{sc}^*/kT)$ for pathways 4A and 4B, respectively, where F is the flux of thiols to the surface, S is a steric factor, θ is the fractional surface coverage, k is Boltzmann's constant, and T is absolute temperature. At the same thiol concentration, the flux F^* is greater than F as mass transport is dominated by a radial or quarterspherical diffusional field for SCSA and a planar diffusional field for the unconstrained self-assembly. Thiols are forced to stand up directly in 4B due to spatial constraint, providing a more favorable configuration for sulfur ligation and a stronger interaction for the chains with the surrounding SAM. These aspects result in a higher sticking/adsorption probability for thiols on gold (i.e., $S^* > S$), and a lower activation energy in SCSA (i.e., $E_{sc}^* < E_2^*$). Therefore, the reaction rate in 4B is faster than that in 4A.

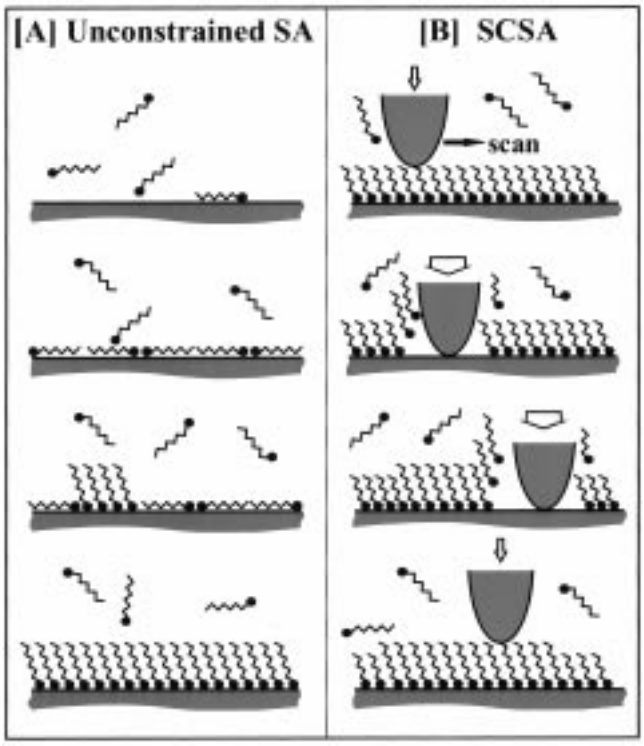

Figure 4. Schematic diagram showing the reaction pathways for the (A) unconstrained and (B) spatially constrained self-assembly (SCSA) reactions. On a bare substrate, the alkanethiols adsorb and cover the gold surface with a lying-down phase that undergoes a transition to the standing-up configuration of the complete monolayer. In SCSA, an AFM tip exposes a bare gold surface within a previously assembled monolayer, and the spatial confinement produced by adsorbed thiols and the AFM tip restricts the formation of a lying-down configuration for adsorbing thiols and instead favors their direct adoption of the standing-up configuration. The small and large arrows above the AFM tip pictorially denote the lower and higher forces applied to the tip for imaging and displacing operations, respectively.

microenvironment fabricated during nanografting. Sufficient spatial confinement can sterically hinder or prevent the thiol molecules from adopting a lying-down phase and instead favor a standing-up configuration. Such a configuration sterically favors direct adsorption of the alkanethiols in a conformation where the sulfurs ligate to gold and the chains pack to form the SAM. In addition, the standing-up configuration is also enthalpically favorable because the interactions between the newly adsorbed molecules and the surrounding thiols help stabilize the transition states for this reaction process. Thus, the overall activation energy for SCSA is most likely lower than that in the unconstrained reaction process. As a result, self-assembly on the constrained gold surfaces proceeds with a faster reaction rate. The proposed model is analogous to the accelerated kinetics observed within the cavities of zeolites and the capsules of certain supramolecular complexes.[11] Investigation into the temperature dependence of the SCSA kinetics and a molecular dynamics simulation of the adsorption process under spatial confinement shall further verify and refine the proposed mechanism.

Conclusions

Using solution-phase self-assembly of thiols onto gold and nanografting, we have demonstrated that the kinetics of SAM formation can be accelerated by producing a transient reaction environment in which gold is spatially confined by surrounding thiols and an AFM tip. This transient microenvironment sterically favors the adoption of a standing-up configuration for the initially adsorbed thiols. Such a spatial confinement effect causes the formation of a self-assembled monolayer to follow a pathway that bypasses the lying-down to standing-up transition found in the corresponding unconstrained reaction. The accelerated kinetics are critically dependent on the dimension of the spatial confinement, with exposed surface dimensions less than the chain length of the adsorbing thiols appearing to prevent alternative reaction paths most efficiently. This finding has generic implications in that spatial confinement can provide an effective means for changing the mechanism of certain surface reactions by sterically hindering alternative pathways and for accelerating the kinetics of a surface reaction by stabilizing particular transition states or reaction intermediates. Such reactions may include surface processes that exhibit similar two-dimensional phase transitions. For instance, 2,5-dimethylthiophene forms a commensurate structure with the thiophene rings lying flat on Au(111), Cu(111), Ni(111), and Pt(111) surfaces at low coverage.[20] As the coverage increases, a herringbone structure forms with the molecular planes tilting away from the surface to accommodate the increased surface density.[20] Other examples include phase transitions in Langmuir monolayers and the behavior of adsorbed polymers and proteins on various surfaces.[21]

Because of its accelerated kinetics and ability to produce scar-free monolayers, spatially confined self-assembly can produce lateral patterns with a nanoscopic to molecular precision. In addition, the fabricated nanostructures can be quickly altered and characterized *in situ*.[12] Potential applications include the ability to produce nanopatterns of receptor groups for the design of chemical and biosensors. With use of pattern transfer protocols,[3] this procedure should allow the fabrication of metal and semiconductor nanostructures for the development of various nanoelectronic devices.

Acknowledgment. We thank Professors W. Hase (Wayne State University) and G. Scoles (Princeton) for many helpful discussions on surface reaction kinetics and dynamics and G. K. Jennings and T.-H. Yong at MIT for the preparation of C_{22}-SH and $C_{18}OC_{19}SH$. G.Y.L. gratefully acknowledges the Camille and Henry Dreyfus Foundation for a New Faculty Award. Both P.E.L. and G.Y.L. are Arnold and Mabel Beckman Young Investigators. S.X. thanks WSU-IMR for a graduate research fellowship. This work was also supported by Wayne State University and the National Science Foundation (CHE-9733400).

JA981938J

(20) (a) Chen, X.; Frank, E. R.; Hamers, R. J. *J. Vac. Sci. Technol. B* **1996**, *14*, 1136. (b) Richardsons, N. V.; Campuzano, J. C. *Vacuum* **1981**, *31*, 449. (c) Schoolf, R.; Preston, R. E.; Benziger, J. B. *Langmuir* **1985**, *1*, 313. (d) Stohr, J.; Gland, J. L.; Kollin, E. B.; Koestner, R. J.; Johnson, A. L.; Mutterties, E. L. *Phy. Rev. Lett.* **1984**, *53*, 2161.

(21) (a) Harkins, W. D.; Boyd, E. *J. Phys. Chem.* **1941**, *45*, 20. (b) Adam, N. K. *Proc. R. Soc. London, Ser. A* **1922**, *101*, 516.